Journal of Zhejiang University-SCIENCE C (Computers & Electronics)
ISSN 1869-1951 (Print); ISSN 1869-196X (Online)
www.zju.edu.cn/jzus; www.springerlink.com
E-mail: jzus@zju.edu.cn

Modeling and noise analysis of a fence structure micromachined capacitive accelerometer system*

Xia ZHANG†1, Hao WANG[1], Xu-dong ZHENG[2], Shi-chang HU[1], Zhong-he JIN[1]

([1]*Department of Information Science and Electronic Engineering, Zhejiang University, Hangzhou 310027, China*)

([2]*Beijing Institute of Aerospace Control Devices, Beijing 100854, China*)

†E-mail: d05zhangxia@zju.edu.cn

Received Dec. 10, 2009; Revision accepted Mar. 26, 2010; Crosschecked Nov. 4, 2010

Abstract: We analyze the effects of possible noise sources on a fence structure micromachined capacitive accelerometer system by modeling and simulation to improve its performance. Simulation results show that a mismatch between the two initial sensing capacitors of the accelerometer or a mismatch between the two capacitance-voltage conversion circuits has a great effect on the output noise floor. When there is a serious mismatch, the noise induced by a sinusoidal carrier is the major noise source. When there is no or only a slight mismatch, the differential capacitance-voltage conversion circuits become the main noise source. The simulation results were validated by experiments and some effective approaches are proposed to improve the system resolution.

Key words: Capacitive accelerometer, Micro-electromechanical system (MEMS), Noise, Modeling, Simulation
doi:10.1631/jzus.C0910757 **Document code:** A **CLC number:** TN304.12

1 Introduction

The use of micro-electromechanical system (MEMS) accelerometers has been reported widely in many areas, such as navigation, seismometry, space microgravity, military affairs, and biomedicine (Yazdi *et al.*, 1998). Capacitive accelerometers have been commonly used because they have several advantages including a low intrinsic temperature coefficient, high sensitivity, low noise, low power dissipation, and are easily integrated with complementary metal oxide semiconductors (CMOS) for monolithic sensing devices (Yun, 1992; Gopel *et al.*, 1994; Yazdi *et al.*, 1998; Wu *et al.*, 2004). To reduce the time and cost from research to market, simulation is commonly used to predict the performance of a sensor system (Lewis and Kraft, 1996; Izham and Ward, 2004; Xue *et al.*, 2005; Mohite *et al.*, 2006). There are two approaches to simulating MEMS sensors. One is system level modeling, which uses differential equations and nonlinear functions. The other is finite element modeling, which can predict the response to forces and moments, and simulate electromagnetic fields and thermodynamic problems (Beeby *et al.*, 2004). Compared with system level modeling, finite element simulation techniques can obtain more realistic simulation results, but it is difficult to simulate entire systems, especially noise components.

Resolution, which is one of the most important parameters in evaluating micromachined accelerometer system performance, can be improved by reducing noise. However, few studies that include almost all the noises in a system level model have been reported.

In this paper, based on Simulink platform, a simulation model of a fence structure micromachined capacitive accelerometer is built to optimize a sensor system. The model includes not only the sensor and the interface circuits, but also all possible noise sources of the system. Simulation results show that a

* Project (No. NCET-06-0514) supported by the Program for New Century Excellent Talents in University of China

mismatch between the two initial sensing capacitors of the accelerometer or a mismatch between the two capacitance-voltage (*C*-*V*) conversion circuits has a great effect on the output noise floor. Based on our conclusions, some appropriate and effective approaches are proposed to improve system resolution.

2 Modeling of a micromachined capacitive accelerometer

A MEMS accelerometer system consists of two main parts, the sensor and the interface circuits. A whole block diagram of a capacitive accelerometer system is shown in Fig. 1. The capacitive accelerometer is fabricated by bulk silicon micromachining technology, so a bulk movable proof-mass can be obtained to reduce the mechanical thermal noise. The accelerometer is composed of a proof-mass suspended by four U-shape springs and fence structure differential capacitors used as the sensing elements. A scanning electron microscope (SEM) view of the accelerometer is shown in Fig. 2a, and the fence structure capacitors can be simplified as shown in Fig. 2b (Zheng *et al.*, 2009). When an acceleration is applied along the *x* axis, the proof-mass (movable fences) will have a displacement, which is transferred into the capacitance variance ΔC by changing the overlapped area rather than the gap. The design not only achieves low damping, but also eliminates the nonlinear effect. As well as the accelerometer, the interface circuits also play a critical role in the overall performance of the system.

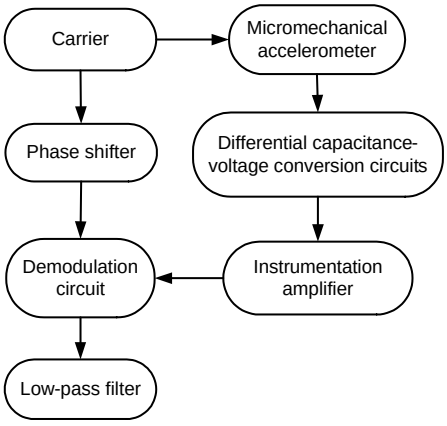

Fig. 1 Schematic of the MEMS accelerometer system

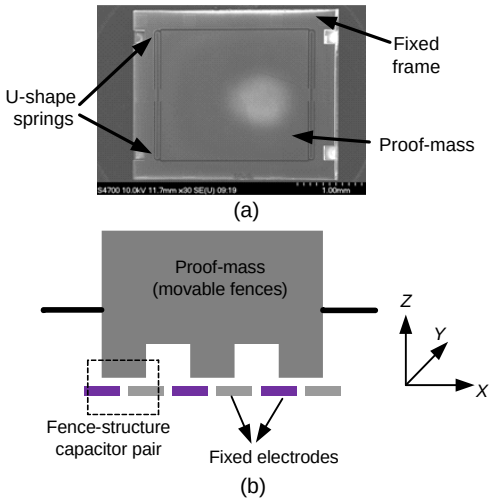

Fig. 2 A scanning electron microscope (SEM) view of a micromachined capacitive accelerometer (a) and the sketch map of the fence structure sensing capacitors (b)

Inertial force due to acceleration will deflect the proof-mass according to Newton's second law. The dynamic equation of the accelerometer is given by

$$m\ddot{\boldsymbol{x}}(t)+b\dot{\boldsymbol{x}}(t)+k\boldsymbol{x}(t)=m\boldsymbol{a}, \tag{1}$$

where $\boldsymbol{x}$ is the displacement of the proof-mass from its rest position with respect to the fixed frame, m is the mass of the proof-mass, $\boldsymbol{a}$ is the acceleration to be measured, k denotes the mechanical spring constant, and b denotes the slide-film damping coefficient. The model of the accelerometer in Simulink was built according to Eq. (1). As a result of manufacturing flaws, there is a mismatch between the two initial sensing capacitors, which will cause a dc bias in the output. There is also a parasitic capacitance, a pad capacitance, and a parasitic resistance in the mechanical structure. These non-ideal factors were all included in the model of the accelerometer.

Many noise sources affect the resolution of an accelerometer system and they all can be classified into two main groups: mechanical and electrical (Kulah and Najafi, 2002). Mechanical- and electrical-thermal noises both result from the Brownian motion of molecules. Mechanical-thermal noise can be modeled as a zero-mean, white Gaussian noise and its power spectral density relates to the mechanical damping of the structure directly (Eq. (2)) (Clark, 1997; Leland, 2005). Electrical-thermal noise can be considered as white noises with a zero-mean

Gaussian distribution (Couch, 1983). Therefore, a Gaussian noise generator is used as a thermal noise in the simulation model.

$$S(\omega)=4K_{\mathrm{B}}Tb,\ \ \omega\geq 0\,, \tag{2}$$

where K_{B}=1.38×10^{-23} J/K is Boltzmann's constant, T is the temperature in Kelvin, b is the slide-film damping coefficient, ω denotes frequency, and $S(\omega)$ denotes the single sided spectral density of the mechanical-thermal noise. For a typical accelerometer with b=1.07×10^{-4} N·s/m and T=300 K, it can be concluded that $S(\omega)$=1.77×10^{-24} N^2/Hz.

The differential C-V conversion circuits and the equivalent half-circuit noise model are shown in Fig. 3.

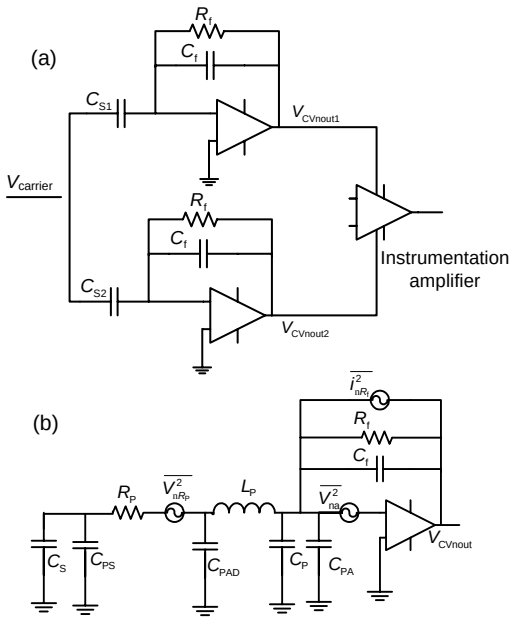

Fig. 3 Capacitance-voltage (C-V) conversion circuits and their equivalent noise model

(a) Differential C-V conversion circuits; (b) Simplified schematic view of equivalent noise

The output equivalent noise voltage can be represented by (Petkov and Boser, 2004)

$$V_{\mathrm{CVnout}}=\sqrt{\left(\frac{C_{\mathrm{T}}}{C_{\mathrm{f}}}\right)^2\overline{V_{\mathrm{na}}^2}+\left(\frac{C_{\mathrm{S}}+C_{\mathrm{PS}}}{C_{\mathrm{f}}}\right)^2\overline{V_{\mathrm{nR_p}}^2}+\left(\frac{1}{2\pi f_{\mathrm{m}}C_{\mathrm{f}}}\right)^2\overline{i_{\mathrm{nR_f}}^2}}\,, \tag{3}$$

where C_{T}=C_{S}+C_{f}+C_{PS}+C_{PAD}+C_{P}+C_{PA}, C_{S} is the sensing capacitance, C_{PS} and R_{P} are the parasitic capacitance and the parasitic resistance, respectively, in the sensor, C_{PAD} is the pad capacitance, C_{P} and L_{P} are the parasitic capacitance and the parasitic inductance, respectively, caused by the non-ideal factors, such as the through vias, between the sensor and the interface circuits, C_{PA} is the input capacitance of the amplifier, C_{f} is the feedback capacitance, R_{f} is the feedback resistance, f_{m} is the carrier frequency, V_{na} is the input-referred noise voltage of the amplifier at f_{m}, $V_{\mathrm{nR_P}}$=$(4K_{\mathrm{B}}TR_{\mathrm{P}})^{1/2}$ represents the thermal noise equivalent voltage of the parasitic resistance, and $i_{\mathrm{nR_f}}$=$(4K_{\mathrm{B}}T/R_{\mathrm{f}})^{1/2}$ represents the thermal noise equivalent current of the feedback resistance. The parameters of a typical fence structure micromachined capacitive accelerometer and a typical amplifier are listed in Table 1.

Table 1 Parameters of a typical accelerometer and a typical amplifier

Parameter	Value
Sensing and parasitic capacitances, C_{S}+C_{PS} (pF)	4
Parasitic resistance, R_{P} (kΩ)	1
Parasitic and pad capacitances, C_{P}+C_{PAD} (pF)	23
Input capacitance, C_{PA} (pF)	2
Feedback capacitance, C_{f} (pF)	10
Parasitic inductance, L_{P} (nH)	1
Feedback resistance, R_{f} (MΩ)	1
Carrier frequency, f_{m} (kHz)	200
Input-referred noise voltage at the carrier frequency, V_{na} (nV/Hz$^{1/2}$)	11

In the micromachined capacitive accelerometer system, the output equivalent noise voltage V_{CVnout} is around 4.4×10^{-8} V/Hz$^{1/2}$ and the test result is shown as the bottom line in Fig. 4. Because the carrier frequency is 200 kHz and the bandwidth of the accelerometer is around 100 Hz, we chose 5–45 Hz as the frequency offset away from the carrier frequency to measure the background noise power spectral density. The noise further away from the carrier frequency would not affect the system resolution because of demodulation and the low-pass filter. The two C-V conversion circuits are realized by dual amplifiers (two in a package), so they have a certain common-mode noise. Owing to the high common-mode rejection ratio (CMRR) of the instrumentation amplifier, common-mode noise can be eliminated and has little effect on the output equivalent noise. Therefore, only the difference-mode noise actually affects the system resolution. The background noise of the instrumentation amplifier is −124 dBm/Hz and the gain equals 22.7 dB. If there is no common-mode noise in the

output equivalent noise of the *C*-*V* conversion circuit, the output equivalent noise voltage of the instrumentation amplifier is around 8.62×10^{-7} V/Hz$^{1/2}$. The output noise floor of the instrumentation amplifier is actually −111.4 dBm/Hz (Fig. 4). Therefore, it can be concluded that the output equivalent difference-mode noise voltage of the *C*-*V* conversion circuit is about 3.16×10^{-8} V/Hz$^{1/2}$.

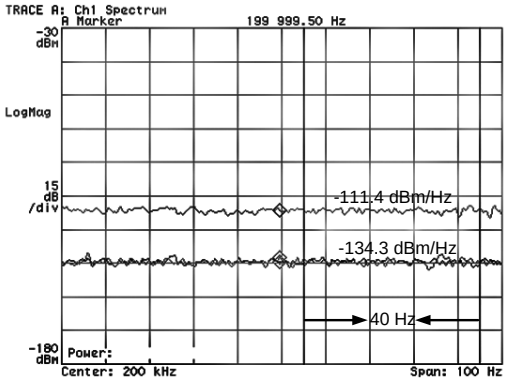

Fig. 4 Test results of the noise floors of the capacitance-voltage (*C*-*V*) conversion circuit and the instrumentation amplifier

The simulation models of other interface circuits were built mathematically according to the transfer functions, except the nonlinear demodulation circuit AD630, which is modeled according to Zhang *et al.* (2008). The electrical-thermal noise, 1/*f* noise, offset voltage, offset voltage drift with temperature, temperature coefficient of resistance, and temperature coefficient of capacitance are included in every circuit model. 1/*f* noise is accomplished using the Fourier filtering method, which can also generate $1/f^{\beta}$ ($0\leq\beta\leq2$). The expression of the *M*-point time sequence $x[n]$ for the Fourier filtering method is given by Eq. (4) (Peitgen and Saupe, 1982). GAUSS(n) represents Gaussian noise and UNIF(n) represents uniform noise.

$$x[n]=\mathrm{RE}\left\{\mathrm{IFFT}\left\{\sum_{n=1}^{M}\mathrm{GAUSS}(n)\cdot n^{-\beta/2}\cdot\left[\cos(2\pi\mathrm{UNIF}(n))+\mathrm{j}\sin(2\pi\mathrm{UNIF}(n))\right]\right\}\right\}. \tag{4}$$

To further validate the noise model, Allan variance was used. Allan variance plots of the test result and the simulation result obtained under constant temperature are shown in Fig. 5. It can be seen that the noise models are accurate, and the system simulation model can reflect the actual system closely. From the test result, it can be concluded that the bias instability is 0.0514 mg, the velocity random walk is 39.1 μg/Hz$^{1/2}$, and the acceleration random walk is 8 μg·Hz$^{1/2}$ by least squares fitting. The bias instability and the acceleration random walk are caused by the ambient temperature drift and the amplitude drift of the carrier wave.

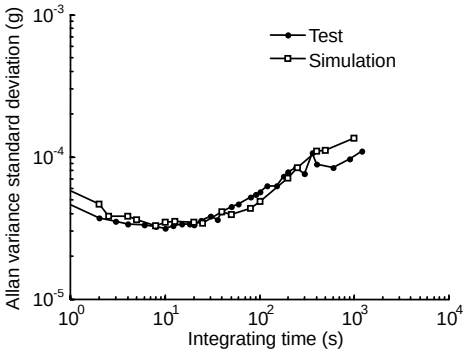

Fig. 5 Allan variance plots of the test and simulation results

Based on the models analyzed above, the system level simulation model of the fence structure micromachined capacitive accelerometer system was built based on the Simulink platform (Fig. 6).

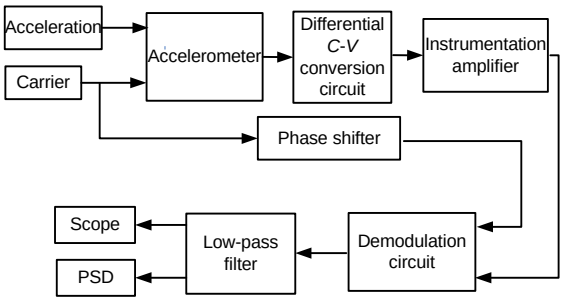

Fig. 6 Simulink block diagram of the fence structure micromachined capacitive accelerometer system
PSD is designed for power spectral density estimation

3 Simulation results and analysis

According to the parameters of a fence structure micromachined capacitive accelerometer and its interface circuit, a simulation model of the accelerometer system with 350 mV/g sensitivity was built. When the input acceleration is zero, there is a dc bias in the output which equals 1.123 V. The sensitivity test of the accelerometer system is performed on a

circular dividing table. By collecting the output data of the system using an Agilent 34401A digital multimeter every 5° and linear data fitting, the system sensitivity is obtained. In the accelerometer system, the amplitude of the input carrier wave is 212 mV; the gains of the instrumentation amplifier and the low-pass filter are 13.67 and 10, respectively. Because the bandwidth of the accelerometer is around 100 Hz, the cutoff frequency of the low-pass filter is designed to be 100 Hz, and we chose the frequency range from 10 Hz to 40 Hz as the integrating interval to calculate the input-referred acceleration noise floor. Fig. 7a shows the frequency spectrum obtained by the PSD block in the simulation model, and it can be seen that the input-referred acceleration noise floor is 33.40 μg/Hz$^{1/2}$. Therefore, the accelerometer system achieves 0.334 mg resolution in 100 Hz bandwidth. The simulation result (Fig. 7b) shows reasonable agreement with the experimental result of 43.38 μg/Hz$^{1/2}$ measured with an HP89441A vector signal analyzer. Because of the imperfect match between the two feedback capacitances or the two feedback resistances in the real circuits, the experimental result is a little higher than the simulation result.

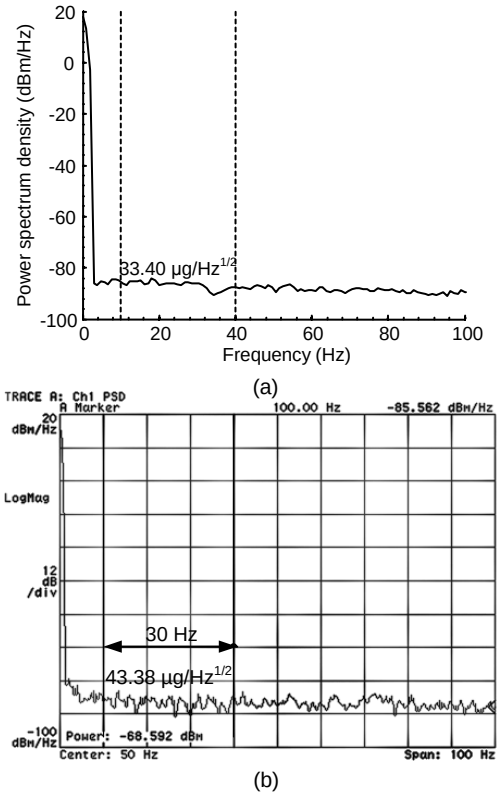

Fig. 7 Output frequency spectrum with zero acceleration input in the simulation (a) and in the experiment (b)

At present, many studies of the noises of accelerometer systems focus on integrating the mathematical expressions of these noises with the given system to evaluate their effects by proximate calculation. However, the method is complex and may not obtain an accurate noise evaluation because of some approximate analyses. For example, the chip AD630 used for demodulation cannot be described simply by an equation. Through the simulation platform, the effect of every noise source on the system performance can be evaluated easily by disabling other noises. The simulation results are listed in Table 2.

Table 2 Simulation results under different mismatching cases (Δ*C*=0.1, 0.3, and 0.7 pF)

Parameter	Value		
	0.1	0.3	0.7
Output noise floor of the system (dBm/Hz)	−88.43	−85.65	−80.60
Input-referred acceleration noise floor (μg/Hz$^{1/2}$)	24.20	33.40	59.62
Percentage of the carrier noise (%)	15.2	55.4	85.8
Percentage of the *C*-*V* conversion circuits' noise (%)	83.7	48.8	18.2

Table 2 shows that the greater the ΔC_S, the higher the output noise floor of the system. The reason is that the mismatch ΔC_S between the two initial sensing capacitors increases the difference-mode noise induced by the carrier. The mismatch between C_{f1} and C_{f2}, or the mismatch between R_{f1} and R_{f2} also has the same effect on the system as ΔC_S.

The differential signal and the total equivalent noise voltage in the output of the differential *C*-*V* conversion circuits can be represented by

$$S_D = \left|[V_c R_{f1} R_{f2}(C_{f2}C_{01} - C_{f1}C_{02})S^2 + V_c(R_{f1}C_{01} - R_{f2}C_{02})S + V_c R_{f1}R_{f2}\Delta C(C_{f1}+C_{f2})S^2 + V_c \Delta C(R_{f1}+R_{f2})S] \cdot [R_{f1}R_{f2}C_{f1}C_{f2}S^2 + (R_{f1}C_{f1}+R_{f2}C_{f2})S+1]^{-1}\right|, \quad (5)$$

$$V_n = \left|\{[(R_{f1}R_{f2}C_{f2} - R_{f1}R_{f2}C_{f1})S^2 + (R_{f1}-R_{f2})S]V_c C_n + [(C_{S1}R_{f1}R_{f2}C_{f2} - C_{S2}R_{f1}R_{f2}C_{f1})S^2 + (R_{f1}C_{S1} - R_{f2}C_{S2})S]V_{cn} + [(R_{f1}R_{f2}C_{f2} - R_{f1}R_{f2}C_{f1})S^2 + (R_{f1}-R_{f2})S]V_{cn}C + [(R_{f1}R_{f2}C_{f2} - R_{f1}R_{f2}C_{f1})S^2 + (R_{f1}-R_{f2})S]V_{cn}C_n\}[R_{f1}R_{f2}C_{f1}C_{f2}S^2 + (R_{f1}C_{f1}+R_{f2}C_{f2})S+1]^{-1}\right| + 2V_{nDM}, \quad (6)$$

where C_n is the equivalent capacitance of the mechanical-thermal noise, V_c is the carrier, V_{cn} is the equivalent noise voltage induced by the carrier, and V_{nDM} is the output equivalent difference-mode noise voltage of one *C*-*V* conversion circuit. The factor of 2 in front of V_{nDM} is due to the differential configuration. From Eq. (5), it can be seen that $V_n=2V_{nDM}$ when $C_{S1}=C_{S2}$, $C_{f1}=C_{f2}$, $R_{f1}=R_{f2}$, so the system noise floor is independent of V_{cn} and C_n. When $C_{S1}\neq C_{S2}$, $C_{f1}\neq C_{f2}$, and $R_{f1}\neq R_{f2}$, V_{cn} and C_n will reduce the system resolution. The output equivalent noise voltage of the whole system is represented by

$$V_{nout}=[(S_D+V_n)G_{IA}+V_{IAn}](\text{switch}(V_c)+V_{cns})G_{LP}+V_{LPn}, \quad (7)$$

where G_{IA} and V_{IAn} are the gain and the output-referred noise voltage of the instrumentation amplifier respectively, and switch(V_c)+V_{cns} represents the AD630's switching operation on the carrier. G_{LP} and V_{LPn} are the gain and the output-referred noise voltage of the low-pass filter, respectively. The mathematical analysis above leads to the same conclusions as in the simulation.

4 Experimental results

The mismatch between the two initial sensing capacitors was around 0.3 pF and the input-referred acceleration noise floor was measured to be 43.38 μg/Hz$^{1/2}$. When the accelerometer was replaced by two ordinary capacitors with a 0.3 pF mismatch, the input-referred acceleration noise floor was 44.20 μg/Hz$^{1/2}$. The difference between the two test results is within the acceptable test error range, so the test results indicate that mechanical-thermal noise has little effect upon the accelerometer system. Therefore, two ordinary capacitors with different values were used as a substitute for the accelerometer, and the output noise floor of the system was measured by increasing the carrier noise. The experimental results are shown in Fig. 8. The *x*-axis 'N_{Vc}' stands for the noise power between 5 Hz and 20 Hz away from the carrier, and the *y*-axis 'N_{out}' stands for the noise power between 10 Hz and 40 Hz in the system output. From Fig. 8, the same conclusion as described above can be reached. ΔC_S has a close relation to the output noise floor of the system, and the greater is the ΔC_S, the more serious is the effect of the carrier noise on the system.

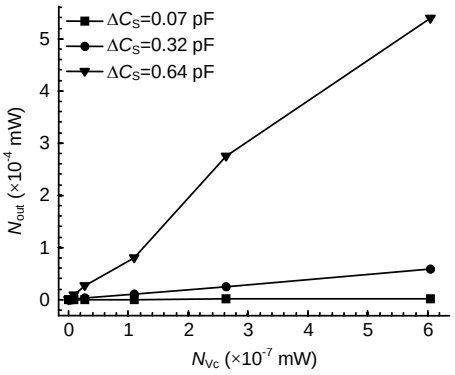

Fig. 8 The system output noise power versus the carrier noise power under different ΔC_S

When the signal-to-noise ratio (SNR) of the carrier is an invariable value, a compensatory capacitance in parallel with the lesser initial sensing capacitor should be adopted to decrease ΔC_S. The ΔC_S caused by micromachining technology errors are between 0.3 pF and 0.8 pF, so the resolution of the micromachined accelerometer system will be improved by this approach.

5 Conclusions

According to the simulation model of the fence structure micromachined capacitive accelerometer system and the experimental results, it can be concluded that compensating the difference of the two initial sensing capacitors of the accelerometer and matching the two capacitance-voltage (*C*-*V*) conversion circuits exactly can not only weaken the effect of the carrier noise, but also improve the system resolution. The differential *C*-*V* conversion circuits then become the main noise source, and the system resolution will be enhanced further by using low-noise amplifiers, without changing the structure of the interface circuits. In the future, a temperature model will be built to analyze its influence on the accelerometer system.

References

Beeby, S., Ensell, G., Kraft, M., Neil, W., 2004. MEMS Mechanical Sensors. Artech House, Boston, USA, p.39-56.

Clark, W.A., 1997. Micromachined Vibratory Rate Gyroscopes. PhD Thesis, University of California, Berkeley,

USA, p.101-104.

Couch, L.W., 1983. Digital and Analog Communication Systems. Prentice Hall, Inc., New Jersey, USA, p.416-594.

Gopel, W., Hesse, J., Zemel, J., 1994. Sensors: a Comprehensive Survey, Vol. 7, Mechanical Sensors. Wiley-VCH, Wienheim.

Izham, Z., Ward, M.C.L., 2004. Dynamic simulation of a resonant MEMS magnetometer in Simulink. *Sens. Actuat. A*, **115**(2-3):392-400. [doi:10.1016/j.sna.2004.04.055]

Kulah, H., Najafi, K., 2002. A Low Noise Switched-Capacitor Interface Circuit for Sub-micro Gravity Resolution Micromachined Accelerometers. Proc. ESSCIRC, p.635-638.

Leland, R.P., 2005. Mechanical-thermal noise in MEMS gyroscopes. *IEEE Sens. J.*, **5**(3):493-500. [doi:10.1109/JSEN.2005.844538]

Lewis, C.P., Kraft, M., 1996. Simulation of a Micromachined Digital Accelerometer in Simulink and PSPICE. UKACC Int. Conf. on Control, p.205-209. [doi:10.1049/cp:19960553]

Mohite, S., Patil, N., Pratap, R., 2006. Design, modeling and simulation of vibratory micromachined gyroscopes. *J. Phys.*, **34**:757-763. [doi:10.1088/1742-6596/34/1/125]

Peitgen, H., Saupe, D., 1982. The Science of Fractal Images. Springer-Verlag, New York, USA, p.93-94.

Petkov, V.P., Boser, B.E., 2004. Capacitive Interfaces for MEMS. *In*: Baltes, H., Brand, O., Fedder, G.K., *et al*. (Eds.), Advanced Micro and Nanosystems. Wiley-VCH, Weinheim, p.49-92.

Wu, J., Fedder, G.K., Carley, L.R., 2004. A low-noise low-offset capacitive sensing amplifier for a 50μg/√Hz monolithic CMOS MEMS accelerometer. *IEEE J. Sol.-State Circ.*, **39**(5):722-730. [doi:10.1109/JSSC.2004.826329]

Xue, W., Wang, J., Cui, T., 2005. Modeling and design of polymer-based tunneling accelerometers by ANSYS/MATLAB. *IEEE/ASME Trans. Mechatr.*, **10**(4):468-472. [doi:10.1109/TMECH.2005.852451]

Yazdi, N., Ayazi, F., Najafi, K., 1998. Micromachined inertial sensors. *Proc. IEEE*, **86**(8):1640-1659. [doi:10.1109/5.704269]

Yun, W., 1992. A Surface Micromachined Accelerometer with Integrated CMOS Detection Circuitry. PhD Thesis, University of California, Berkeley, USA.

Zhang, X., Zheng, X.D., Zheng, Y.M., Luo, S.J., Wang, Y.L., Jin, Z.H., 2008. A new modeling method of MEMS system's noise. *Chin. J. Sens. Actuat.*, **21**(3):498-500 (in Chinese).

Zheng, X.D., Jin, Z.H., Wang, Y.L., Lin, W.J., Zhou, X.Q., 2009. An in-plane low-noise accelerometer fabricated with an improved process flow. *J. Zhejiang Univ.-Sci. A*, **10**(10):1413-1420. [doi:10.1631/jzus.A0820757]

2009 JCR of Thomson Reuters for *JZUS-A* and *JZUS-B*

ISI Web of Knowledge℠

Journal Citation Reports®

WELCOME | HELP | RETURN TO LIST | PREVIOUS JOURNAL | NEXT JOURNAL

2009 JCR Science Edition

Journal: Journal of Zhejiang University-SCIENCE B

Mark	Journal Title	ISSN	Total Cites	Impact Factor	5-Year Impact Factor	Immediacy Index	Citable Items	Cited Half-life	Citing Half-life
☐	J ZHEJIANG UNIV-SC B	1673-1581	619	1.041		0.156	128	3.1	7.5

Journal: Journal of Zhejiang University-SCIENCE A

Mark	Journal Title	ISSN	Total Cites	Impact Factor	5-Year Impact Factor	Immediacy Index	Citable Items	Cited Half-life	Citing Half-life
☐	J ZHEJIANG UNIV-SC A	1673-565X	322	0.301		0.066	213	3.0	6.8

JZUS-A is an international "Applied Physics & Engineering" reviewed-Journal, covering research in Applied Physics, Mechanical and Civil Engineering, Environmental Science and Energy, Materials Science, and Chemical Engineering. *JZUS-B* is an international "Biomedicine & Biotechnology" reviewed-Journal, covering research in Biomedicine, Biochemistry, and Biotechnology. *JZUS-A* and *JZUS-B* were covered by SCI-E in 2007 and 2008, respectively. This is the first time that both journals have gained the Impact Factor.